Science Advances
AAAS

Supplementary Materials for

Reversibly photoswitchable protein assemblies with collagen affinity for in vivo photoacoustic imaging of tumors

Shuai Chen *et al.*

Corresponding author: Peng Huang, peng.huang@szu.edu.cn

Sci. Adv. **10**, eadn8274 (2024)
DOI: 10.1126/sciadv.adn8274

This PDF file includes:

Figs. S1 to S16

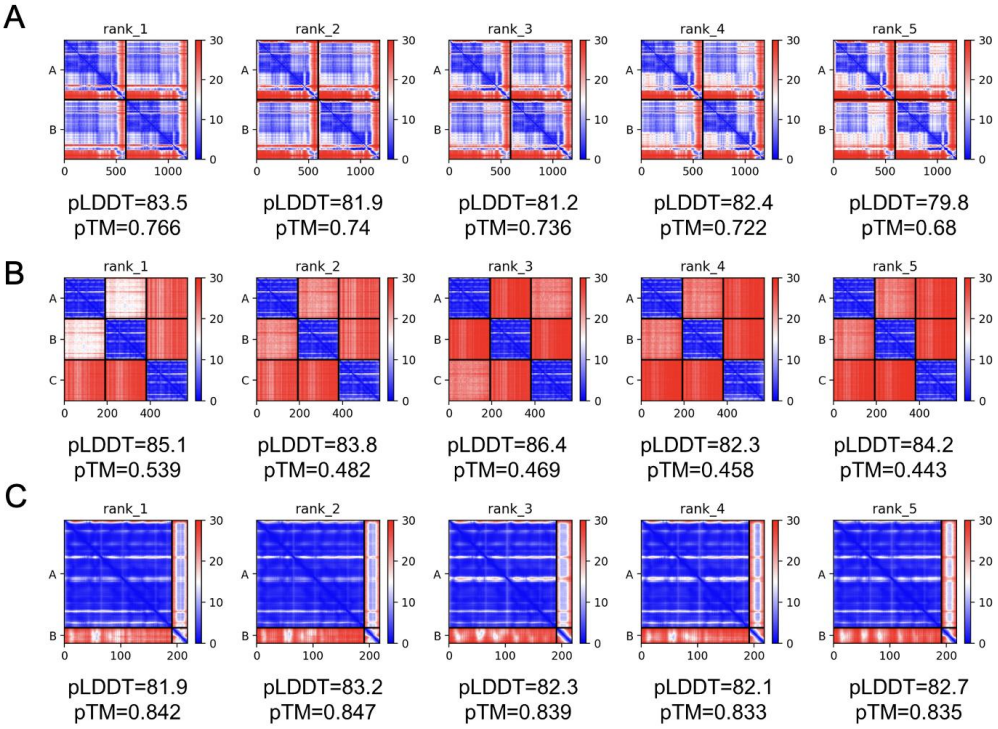

Fig. S1. Structural prediction accuracy for AlphaFold2 models. This heat map displays Predicted Alignment Errors (PAE) in angstroms for AlphaFold2 models, illustrating deviations across residue pairs in: (A) DrBphP (residues 1-594), a stable dimer; (B) CBD (residues 1683-1873), a stable trimer; and (C) CBD's interaction with collagen I. Included are the Predicted Local Distance Difference Test (pLDDT) scores and predicted template modeling (pTM) scores.

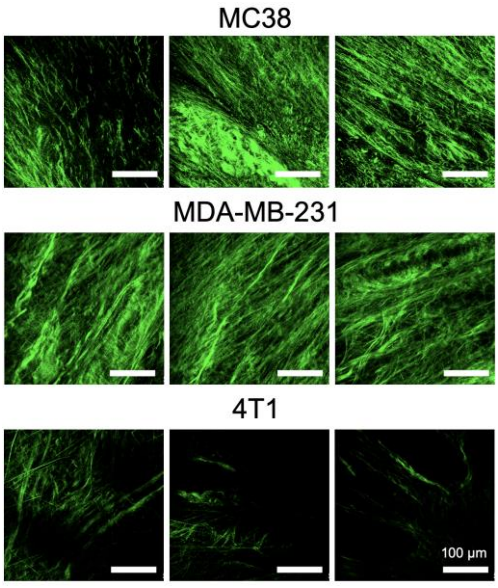

Fig. S2. Collagen distribution in tumors via *in vivo* Second-harmonic generation (SHG) imaging. SHG images showcase collagen content within three different tumor phenotypes. Scale bar is 100 µm.

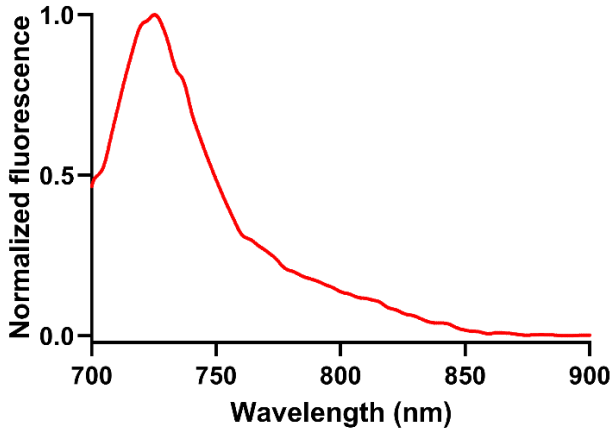

Fig. S3. Fluorescence emission spectrum of DrBphP-CBD. Normalized fluorescence spectrum of DrBphP-CBD (λ_{ex} = 684 nm, λ_{em} = 725 nm).

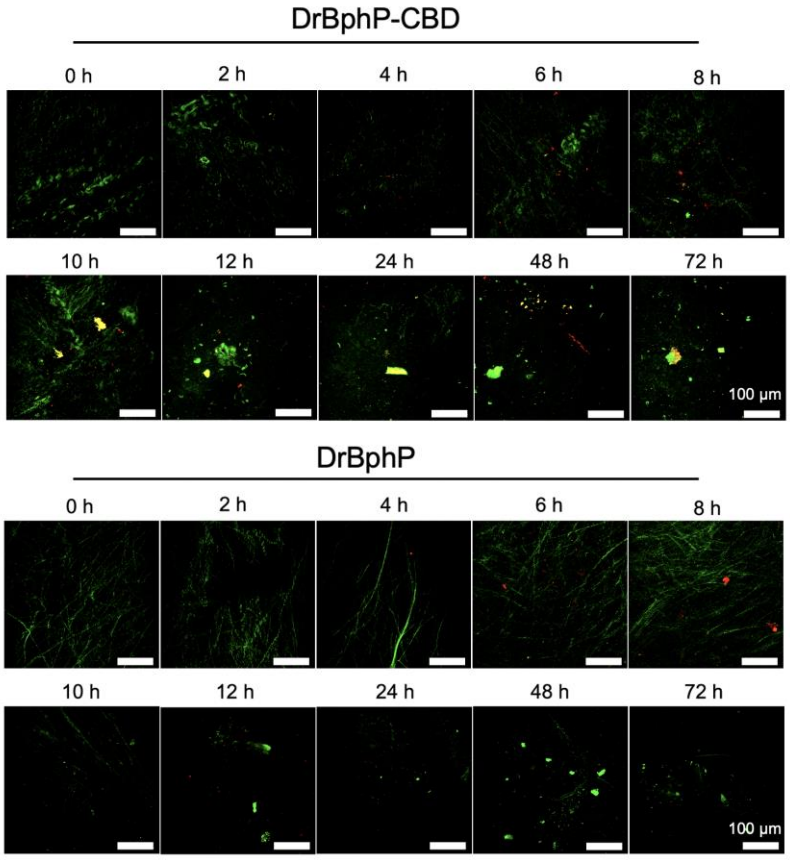

Fig. S4. Serial *in vivo* imaging of 4T1 tumors treated with DrBphP-CBD or DrBphP. Tracking DrBphP-CBD and DrBphP accumulation in 4T1 tumors, paired with collagen visualization via SHG. Scale bar is 100 µm.

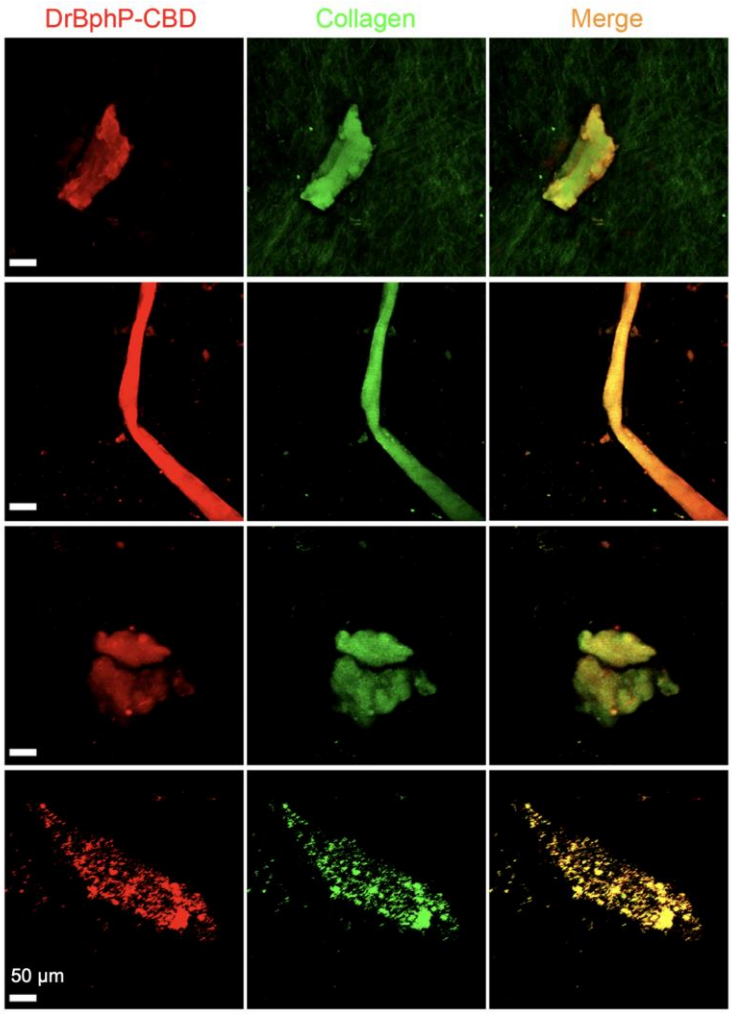

Fig. S5. Intravital microscopy visualization of MC38 tumors. DrBphP-CBD's colocalization with collagen in MC38 tumors, with collagen detection via SHG. Scale bar is 50 μm.

A

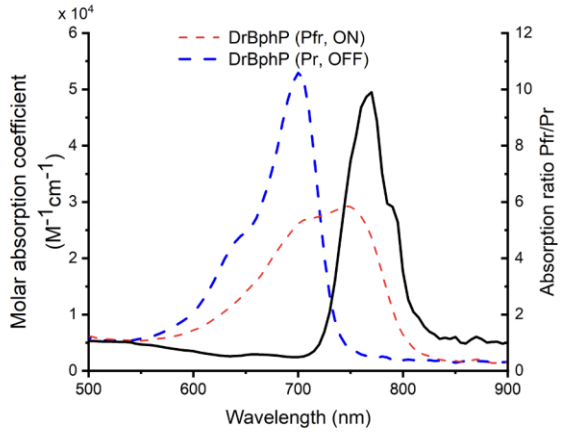

B

Protein	Molar absorption coefficient at 760 nm (10^4 $M^{-1}cm^{-1}$)		
	ON state	OFF state	Photoswitching ratio (ON/OFF)
DrBphP-CBD	2.832	0.263	10.76
DrBphP	2.74	0.293	9.35

Fig. S6. Comparison of absorption spectra and photoswitching properties between DrBphP-CBD and DrBphP. (A) Molecular absorption spectra for DrBphP in ON (Pfr) and OFF (Pr) states, modulated by 808 nm and 635 nm light, respectively. The absorption coefficient ratio at 760 nm is approximately 9.35. (B) Comparative analysis of the absorption states and absorption ratio of DrBphP-CBD and DrBphP, demonstrating comparable absorption spectra and photoswitching efficiencies.

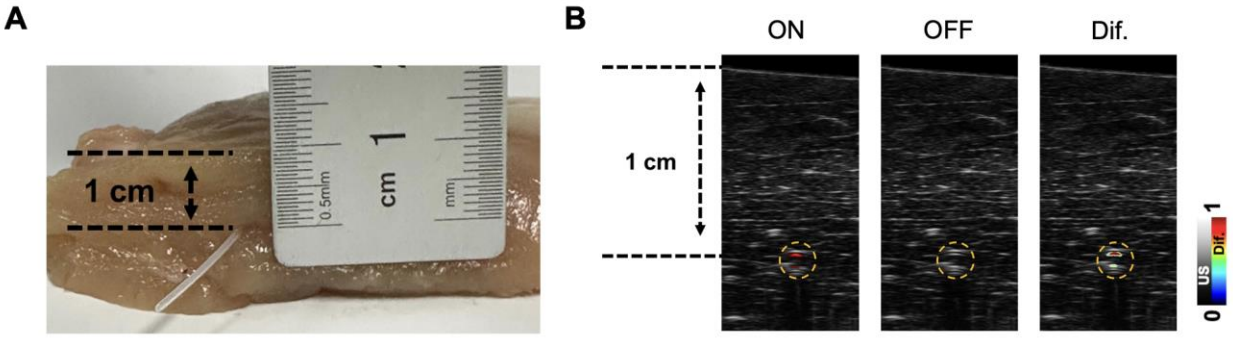

Fig. S7. Photoacoustic evaluation of DrBphP-CBD in chicken breast tissue. (A) Photograph of a plastic tube containing DrBphP-CBD (0.2 mM) embedded at a depth of 1 cm in chicken breast tissue. (B) Photoacoustic B-scan of the phantom in ON, OFF, and their differential responses, overlaid on the ultrasound (US) image, triggered by 760 nm photo-illumination to induce photoswitching.

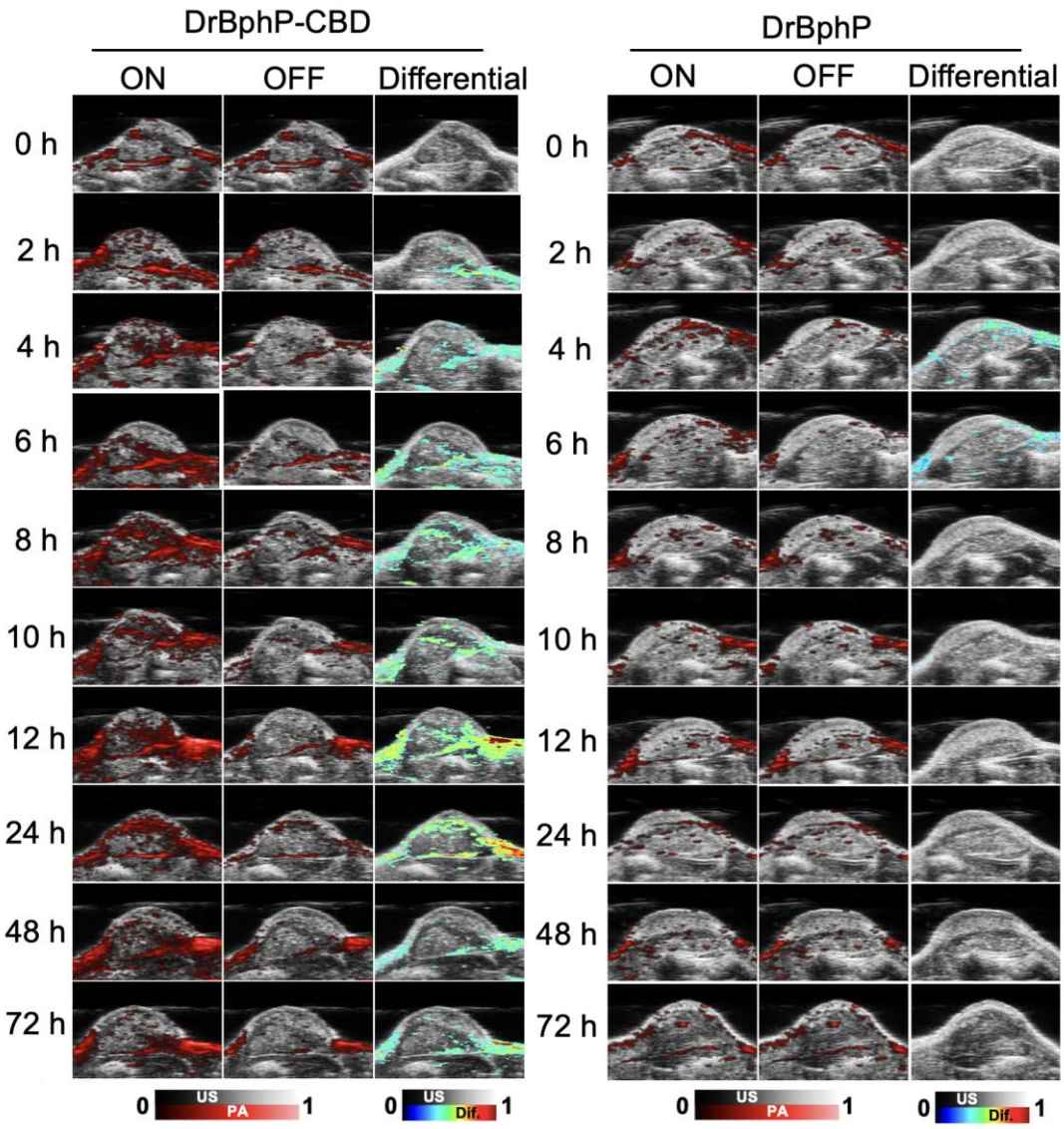

Fig. S8. PA/US images of MDA-MB-231 tumor treated with DrBphP-CBD. Sequential captures of ON, OFF, and differential states of DrBphP-CBD and DrBphP in MDA-MB-231 tumors.

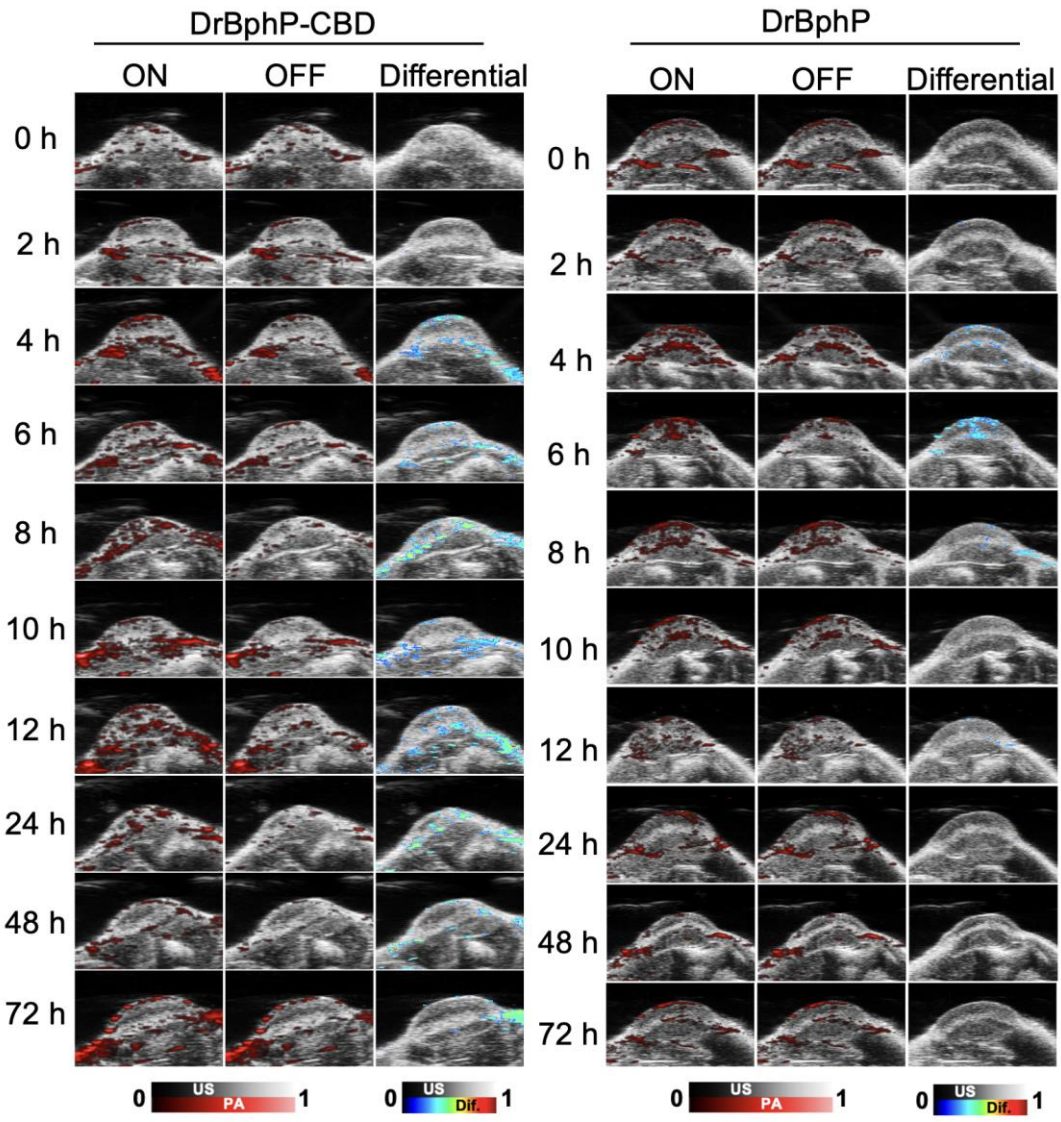

Fig. S9. Time-series PA/US images of 4T1 tumors treated with DrBphP-CBD or DrBphP. Capturing ON, OFF, and differential states of DrBphP-CBD and DrBphP in 4T1 tumors.

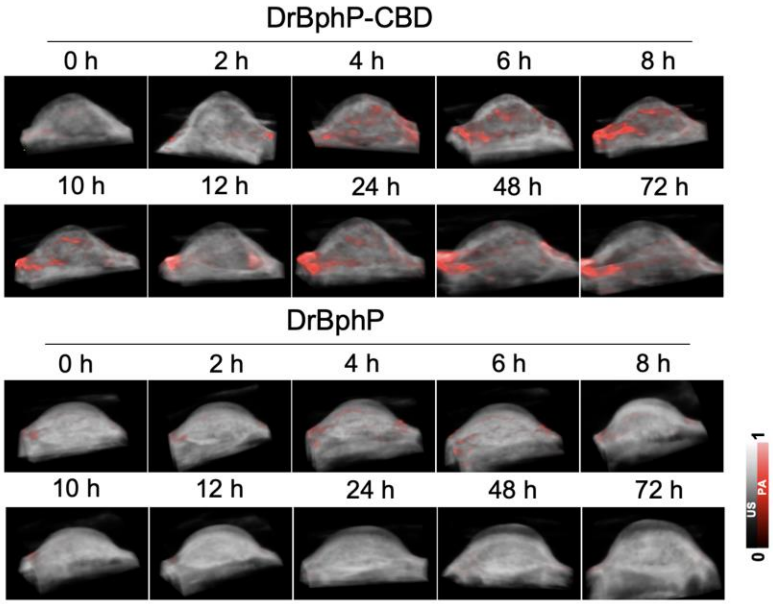

Fig. S10. 3-D PA/US images at 715 nm of MDA-MB-231 tumors treated with DrBphP-CBD or DrBphP. 3-D images of DrBphP-CBD and DrBphP at specific time points in MDA-MB-231 tumors.

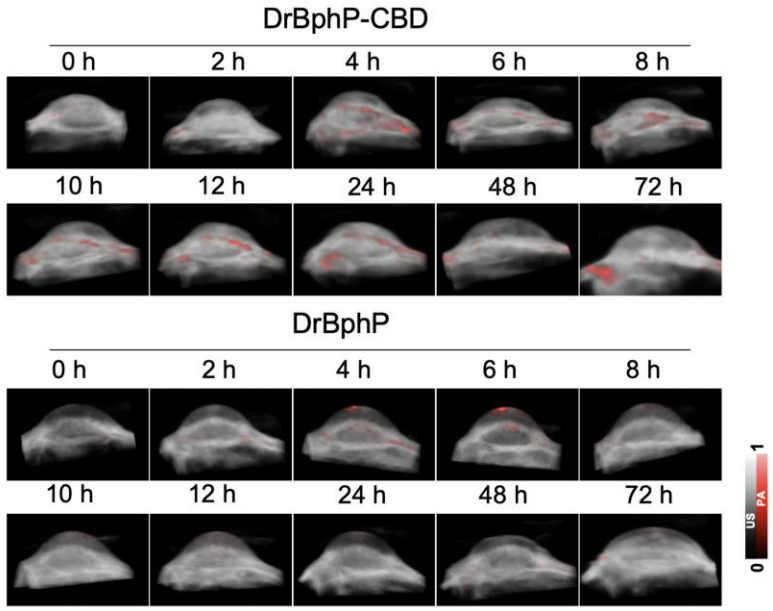

Fig. S11. 3-D PA/US images at 715 nm of 4T1 tumors treated with DrBphP-CBD or DrBphP. 3-D images of DrBphP-CBD and DrBphP at specific various time intervals in 4T1 tumors.

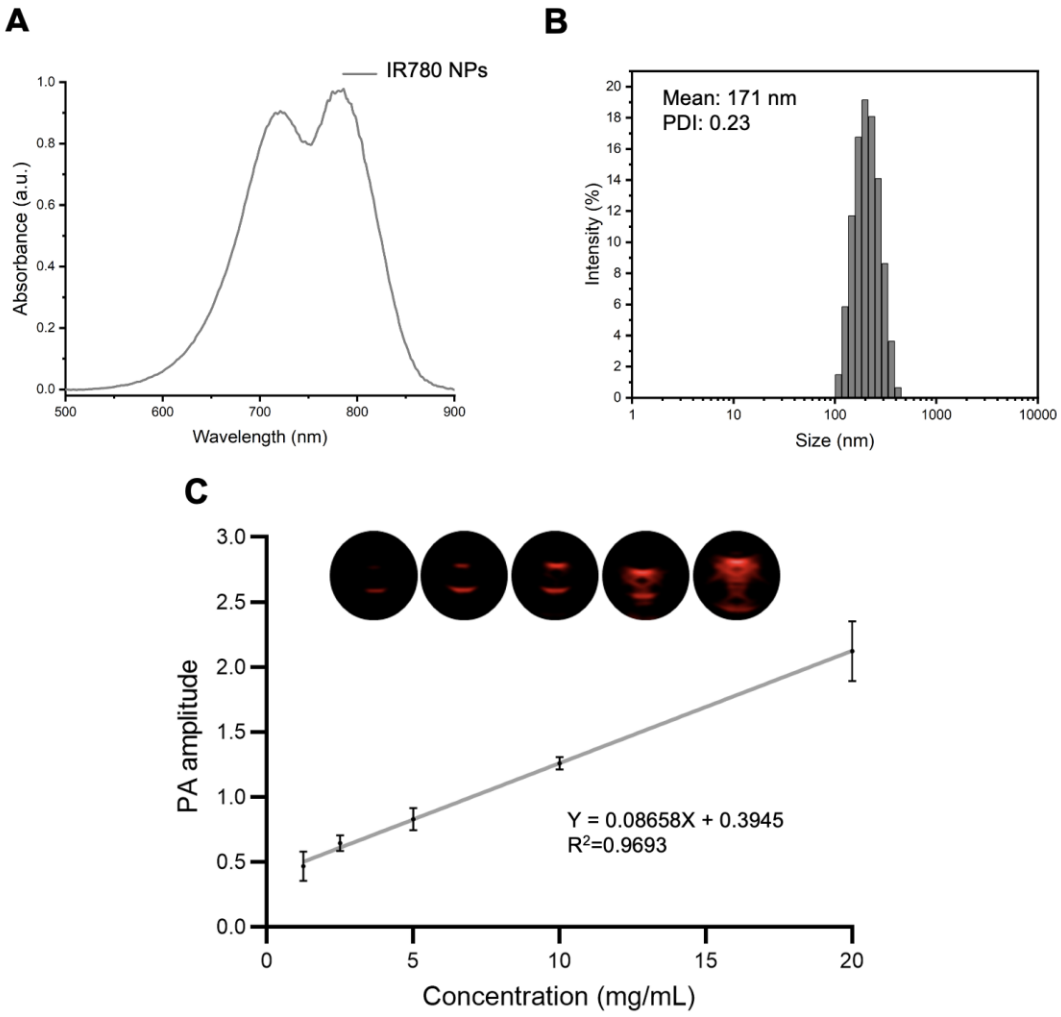

Fig. S12. Characterization of IR780 NPs. (A) UV-vis absorbance spectrum of IR780 NPs dispersed in water. (B) Measurement of the average hydrodynamic diameter of IR780 NPs using dynamic light scattering (DLS). (C) *In vitro* PA images of IR780 NPs at various concentrations along with linear regression fits depicting the relationship between PA amplitude and concentration at a wavelength of 780 nm.

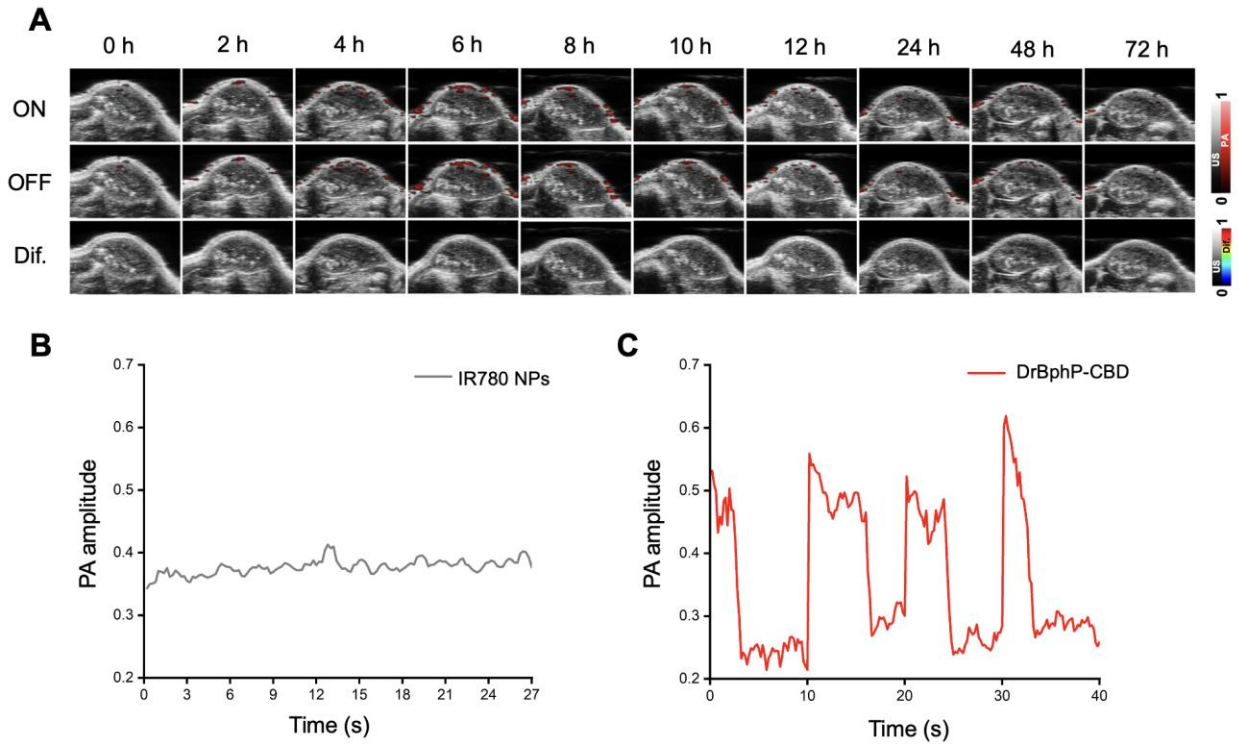

Fig. S13. *In vivo* PA images of MC38 tumors treated with IR780 NPs. (A) Sequential PA/US images at 780 nm demonstrated that the lack of photoswitching ability in IR780 results in identical PA signals within tumor regions for both the "OFF" and "ON" states, leading to a differential PA signal of zero. (B) PA signal of IR780 NPs localized in MC38 tumor regions, captured 6 h post-injection, remained constant upon exposure to 780 nm laser pulses. (C) PA signal switching dynamics of MC38 tumors treated with DrBphP-CBD, observed at 6 h post-injection. The transition from ON to OFF state could be completed within 6 s during data collection at 760 nm. Following this, irradiation with a 635 nm laser for 10 s post-OFF state achieved full reversion to the ON state.

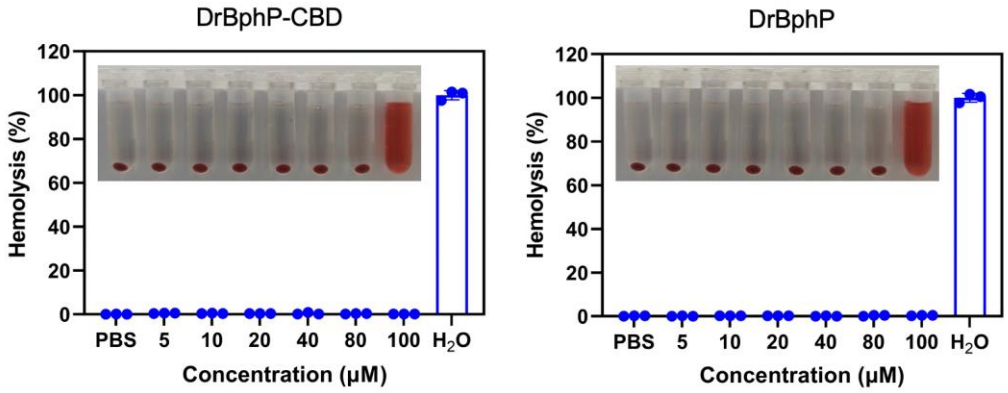

Fig. S14. Hemolysis assay of DrBphP-CBD and DrBphP. Evaluating hemolytic activity of DrBphP-CBD and DrBphP at varing concentrations.

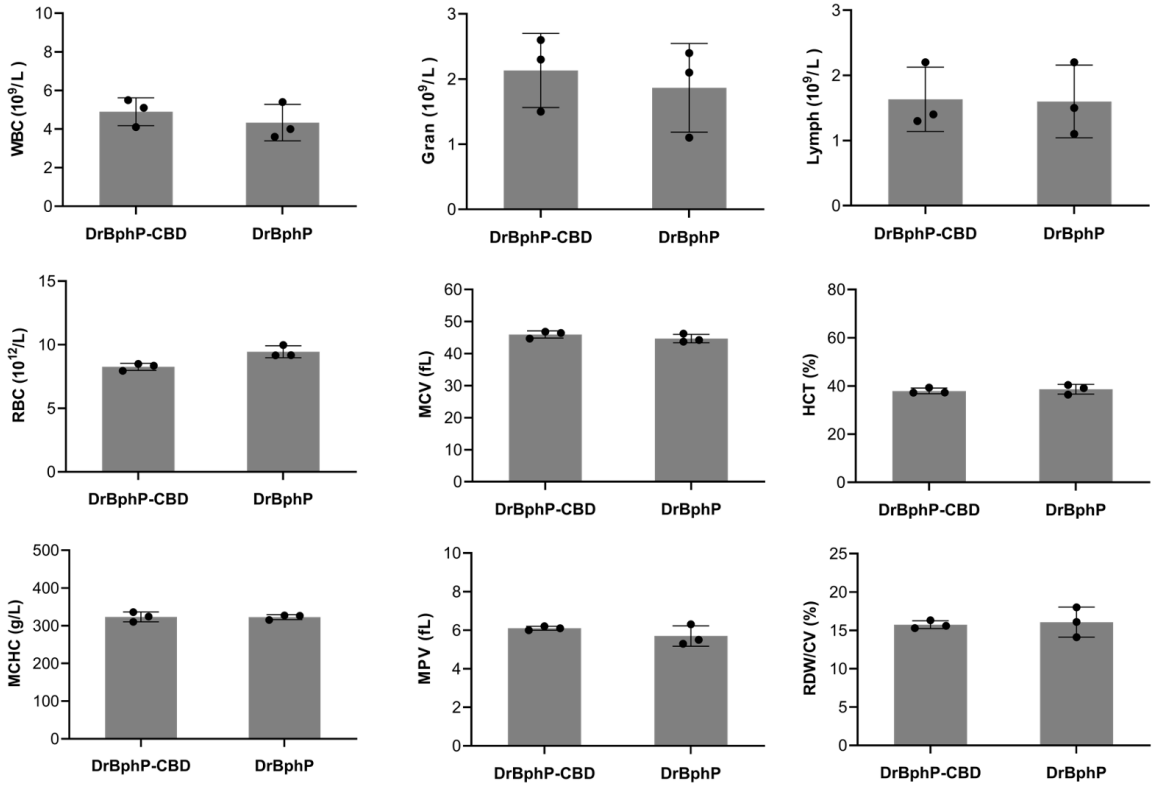

Fig. S15. Blood parameter analysis of mice treated with DrBphP-CBD or DrBphP. Examining blood parameters 7 days after intravenous administration of DrBphP-CBD and DrBphP. Data are presented as mean ± SD (n=3).

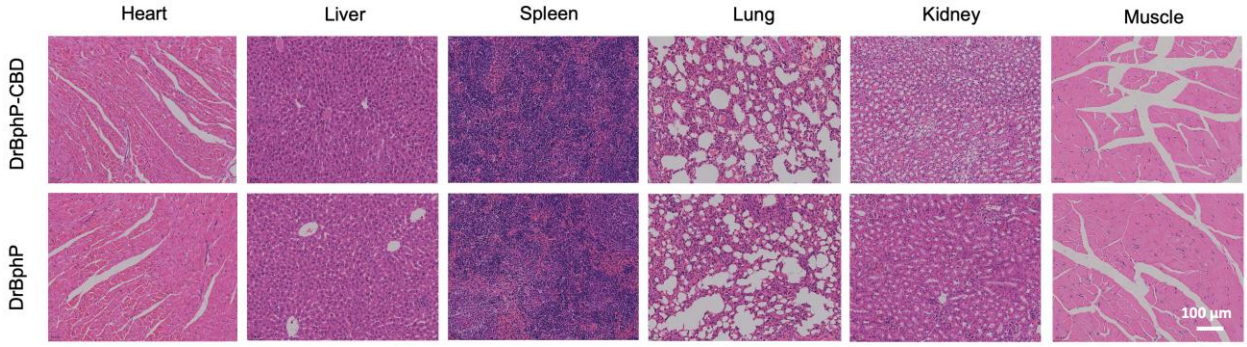

Fig. S16. Histological examination of mice treated with DrBphP-CBD or DrBphP. H&E staining images of tissue sections from major organs and muscle extracted from mice 7 days after intravenous injection of DrBphP-CBD or DrBphP.